



OXFORD CENTRE FOR COLLABORATIVE APPLIED MATHEMATICS

Report Number 11/31

The indentation of pressurized elastic shells: From polymeric capsules to yeast cells

by

Dominic Vella, Amin Ajdari, Ashkan Vaziri and Arezki Boudaoud



Oxford Centre for Collaborative Applied Mathematics
Mathematical Institute
24 - 29 St Giles'
Oxford
OX1 3LB
England

The indentation of pressurized elastic shells: From polymeric capsules to yeast cells

Dominic Vella^{1,2}, Amin Ajdari³, Ashkan Vaziri³ and Arezki Boudaoud⁴

¹*Department of Applied Mathematics and Theoretical Physics,*

University of Cambridge, Wilberforce Road, Cambridge, CB3 0WA, UK

²*OCCAM, Mathematical Institute, University of Oxford, 24-29 St Giles', Oxford, OX1 3LB, UK*

³*Department of Mechanical and Industrial Engineering,*

Northeastern University, Boston, MA, 02115, USA

⁴*Laboratoire Reproduction et Développement des Plantes & Laboratoire Joliot-Curie, INRA, CNRS, ENS, Université de Lyon, 46 Allée d'Italie, F-69364 Lyon Cedex 07, France*

Pressurized elastic capsules arise at scales ranging from the 10 m diameter pressure vessels used to store propane at oil refineries to the microscopic polymeric capsules that may be used in drug delivery. Nature also makes extensive use of pressurized elastic capsules: plant cells, bacteria and fungi have stiff walls, which are subject to an internal turgor pressure. Here we present theoretical, numerical and experimental investigations of the indentation of a linearly elastic shell subject to a constant internal pressure. We show that, unlike unpressurized shells, the relationship between force and displacement demonstrates two linear regimes. We determine analytical expressions for the effective stiffness in each of these regimes in terms of the material properties of the shell and the pressure difference. As a consequence, a single indentation experiment over a range of displacements may be used as a simple assay to determine both the internal pressure and elastic properties of capsules. Our results are relevant for determining the internal pressure in bacterial, fungal or plant cells. As an illustration of this, we apply our results to recent measurements of the stiffness of baker's yeast and infer from these experiments that the internal osmotic pressure of yeast cells may be regulated in response to changes in the osmotic pressure of the external medium.

Keywords: finite element method; buckling; turgor regulation; cell wall

I. INTRODUCTION

Just as one might ‘poke’ an object to have a qualitative sense of its material properties, materials scientists often use an indentation test to make quantitative measurements of an object's elasticity^{1–3}. Indentation is a useful technique because it is repeatable and non-destructive. For small scale applications in biology, it is common to use an Atomic Force Microscope (AFM) in an indentation test to obtain high levels of accuracy that would not otherwise be possible⁴. While several studies have focussed on determining the mechanical properties of both animal and plant cells using variants of the indentation test^{5,6}, a question of particular interest for plant, fungal and bacterial cells is the turgor pressure within the cell. Indeed, differences in turgor pressure could be important for the regulation of growth⁷. It has been suggested previously^{8–11} that indentation using an AFM would allow the turgor pressure of bacteria to be measured. However, this previous work relied on an *ad hoc* approach to the equations of elasticity rather than using classical shell theory.

From a fundamental point of view, the indentation of unpressurized elastic shells has received a great deal of theoretical attention^{12–15}. Much of the early work focused on axisymmetric geometries but more recently the simple problem of indentation has been used as a starting point to understand some of the more complicated geometries that arise when an object with an intrinsic curvature is subject to different external loads^{16,17}. In contrast, very little work has concerned the indentation of a pressurized elastic shell, despite its technological im-

portance in applications such as pressure vessels¹⁸ or capsules designed for drug delivery^{19,20}. However, numerical simulations have been carried out for the case of a thick, fluid-filled shell with a constant volume²¹ and for a thin shell (or membrane) subject to a constant internal pressure²⁰.

Here we carry out a comprehensive investigation of the indentation of spherical pressurized shells, combining an analytical study of the equations of shells with finite element simulations and macroscopic experiments. After the formulation of the problem of interest, we successively focus on the regimes of small and large indentations. We show that in each of these regimes the shell has a characteristic stiffness and determine analytical expressions for these stiffnesses in terms of the material properties of the system. Finally, we apply these results to previous microscopic experiments on the indentation of polymeric capsules²⁰ and of baker's yeast²². In particular, our approach allows us to investigate the regulation of the osmotic pressure of yeast cells.

II. FIRST OBSERVATIONS AND FORMULATION

Our model system is shown schematically in figure 1a. We consider an elastic shell of natural radius R , thickness h , Young's modulus E , Poisson ratio ν that is subject to an internal pressure (or pressure difference) p . The shell is then deformed by the action of a point-like force, F . Numerical simulations were performed using the commercial finite element package ABAQUS (SIMU-

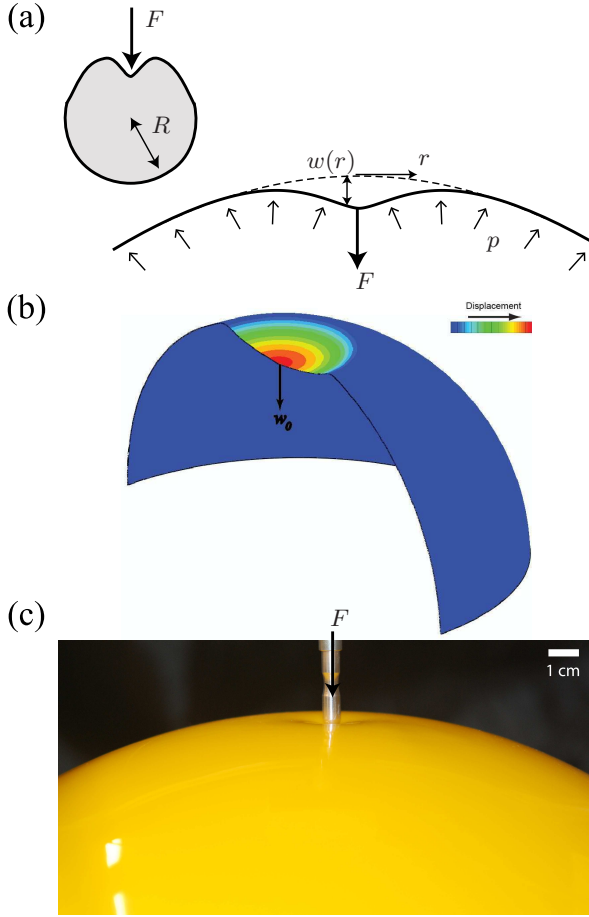


FIG. 1. (Online version in colour.) The indentation of an inflated spherical shell considered here. (a) Idealized setup and notation for the problem: a spherical shell of thickness h and undeformed radius R is subject to an internal pressure, p , while also being loaded by a vertical point force F at a pole. This causes a vertical deflection $w(r)$ and, in particular, a displacement $w(0) = -w_0$ at the point of application of the force. (b) Three-dimensional cross-section of a deformed shell with $w_0 = 13$ cm from numerical simulations with $E = 70$ GPa, $\nu = 0.3$, $R = 1$ m, $h = 2$ mm and $p = 10^4$ Pa. (c) Image showing the experimental setup in which a Pezzi ball (Ledragomma) is inflated and loaded by an indenter.

LIA, Providence, RI), a commercial finite element package, with material properties $R = 1$ m, $E = 70$ GPa and $\nu = 0.3$. (Three-node thin quadratic axisymmetric shell elements were used in all calculations and a mesh sensitivity study was carried out to ensure that the results are minimally sensitive to the element size.) To simulate the response of a pressurized shell, a uniform internal pressure was first applied to the shell. A point load was then applied, while the internal pressure was kept constant, and the relationship between applied force F and maximum displacement w_0 was determined for a range of internal pressures and shell thicknesses. An image of the deformed shell from simulations is shown in figure 1b.

Two typical force-displacement curves are shown in

figure 2a. The first curve shows the force-displacement curve in the absence of an internal pressure. In this case we recover the two classical results for an unpressurized shell: for $w_0 \ll h$, $F \sim w_0$, as shown by Reissner¹³, while for $w_0 \gg h$, $F \sim w_0^{1/2}$ as shown by Pogorelov¹⁴. However, with an internal pressure the results in figure 2a show that there are two separate linear regimes. Further analysis reveals that the prefactor of this linear relationship in the first regime, k_1 , differs from that in the unpressurized case. In this article we focus on understanding the presence of these linear regimes and determining the two linear stiffnesses, k_1 and k_2 , in terms of the material properties of the system.

In order to test the experimental applicability of our approach, we also performed a series of indentation tests using an inflated rubber ball (Pezzi ball, Ledragomma) of radius $R = 18.5$ cm, shell thickness $h = 1$ mm. The Young's modulus was measured to be $E = 2.3$ MPa (by determining the linear relationship between internal pressure and shell circumference) and we assume that the Poisson ratio $\nu = 0.5$, as is typical of rubbers. The ball was inflated to a known pressure and then loaded using a hemispherical cap indenter (see figure 1c) at a constant speed. (The radius of curvature of the indenter ≈ 3 mm, which is significantly smaller than the horizontal length scale for the deformation of the shell $\gtrsim 3$ cm making this a satisfactory approximation to the point force assumed theoretically. Experiments were conducted at room temperature and the ball was supported by a wooden shelf with a cut-out hole to ensure alignment of the pole with the indenter.) The force required to impose this displacement was measured continuously using a force gauge (Andilog centor). Force-displacement curves for a range of internal pressures demonstrate that for small displacements the measured force is approximately linear in displacement with a prefactor that depends on the internal pressure (fig. 2b).

For the theoretical formulation of the problem, we start from the equations of axisymmetric plate theory modified to incorporate the finite radius of curvature of the shell. These equations are well-known²³ and, in the polar geometry of interest here, take the form

$$B\nabla^4 w + \frac{1}{R} \frac{1}{r} \frac{d}{dr} (r\psi) - \frac{1}{r} \frac{d}{dr} \left(\psi \frac{dw}{dr} \right) = p - \frac{F}{2\pi} \frac{\delta(r)}{r} \quad (1)$$

and

$$\frac{1}{Eh} \frac{1}{r} \frac{d}{dr} \left\{ r \frac{d}{dr} \left[\frac{1}{r} \frac{d}{dr} (r\psi) \right] \right\} = \frac{1}{R} \nabla^2 w - \frac{1}{2r} \frac{d}{dr} \left(\frac{dw}{dr} \right)^2 \quad (2)$$

where $w(r)$ is the vertical displacement of the membrane (from the spherical state) and ψ is the derivative of the Airy stress function so that $\sigma_{\theta\theta} = \psi'$ and $\sigma_{rr} = \psi/r$. We use a Dirac δ -function to represent the point forcing at the origin and have chosen the sign convention so that positive F acts in the opposite direction to the pressure, p . We thus expect positive forces to produce negative displacements.

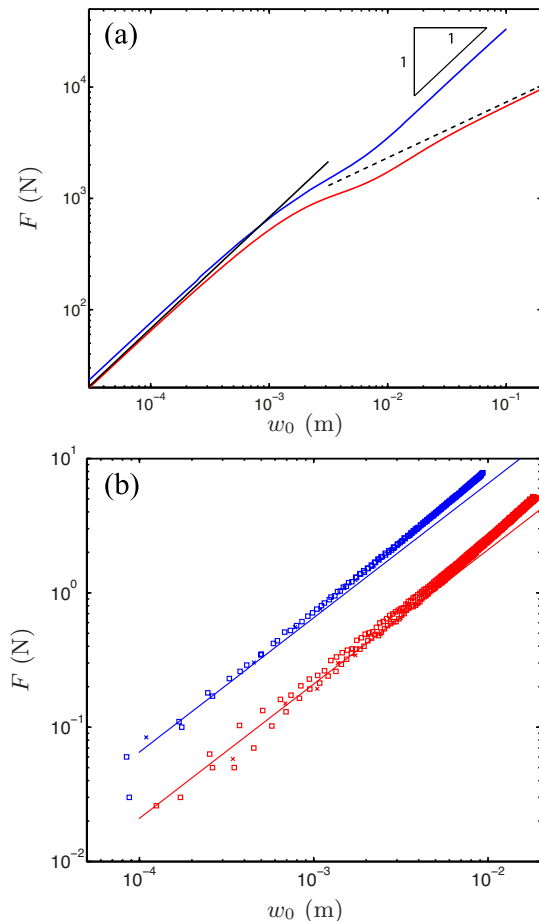


FIG. 2. (Online version in colour.) Force-displacement curves in indentation tests. (a) In the absence of a pressure difference, $p = 0$ (red curve) the numerical results recover the asymptotic results of Reissner¹³ (solid line) and Pogorelov¹⁴ (dashed line). However, with $p = 10^5$ Pa (blue curve), a new linear regime is observed at large displacements. Here $E = 70$ GPa, $\nu = 0.3$, $R = 1$ m, $h = 2$ mm. (b) Experimental results obtained with a Pezzi ball with internal pressure $p = 1.2$ kPa (red) and $p = 5.4$ kPa (blue). Results are shown for loading at a speed of $200 \mu\text{m/s}$ (squares) and unloading at $1000 \mu\text{m/s}$ (crosses). In each case two runs are shown with every twentieth point plotted. The lack of a significant discrepancy between repeated experiments demonstrates the reproducibility of our results as well as the unimportance of frictional and rate effects. The two solid lines represent the linear force laws $F = k_1 w_0$ with the appropriate value of k_1 predicted by theory (see §III).

III. SMALL INDENTATION

For the case of no applied point force, $F = 0$, we anticipate that $w = w_\infty$, a constant. Substituting this ansatz into (1) we find that

$$\psi = pRr/2. \quad (3)$$

The shell is therefore in a uniform state of stress in which $\sigma_{\theta\theta} = \sigma_{rr} = \sigma_\infty = pR/2$. To consider small deformations from this state, it is natural to perturb the base state

given by (3) letting $w \rightarrow w + w_\infty$ and $\psi \rightarrow \psi + \sigma_\infty r$. At leading order, we eliminate ψ from (1) by using (2) to find that the displacement of the shell is governed by

$$B\nabla^4 w - \sigma_\infty \nabla^2 w + \frac{Eh}{R^2} w = -\frac{F}{2\pi} \frac{\delta(r)}{r}. \quad (4)$$

We note that a balance between the term representing bending and the linear restoring force gives rise to a natural bending length scale,

$$\ell_b = \left(\frac{BR^2}{Eh} \right)^{1/4} \sim (hR)^{1/2}. \quad (5)$$

The appropriate solution of (4) subject to $w(0) = -w_0$ is

$$w(r) = -\frac{2w_0}{\log(\lambda_-/\lambda_+)} \left[K_0(\lambda_+^{1/2} r/\ell_b) - K_0(\lambda_-^{1/2} r/\ell_b) \right], \quad (6)$$

where

$$\begin{aligned} \lambda_\pm &= \tau \pm (\tau^2 - 1)^{1/2}, \\ \tau &= \frac{1}{2}\sigma_\infty \left(\frac{R^2}{EhB} \right)^{1/2} = \frac{1}{4}pR^2 (EhB)^{-1/2} \end{aligned} \quad (7)$$

and $K_0(x)$ is the modified Bessel function of zeroth order²⁴. We note that the coefficients of the K_0 terms in (6) are chosen such that there is no logarithmic singularity close to the point of indentation. The parameter τ represents a dimensionless pressure. It is a simple matter to calculate the force by integrating (4) once to give $F = k_1 w_0$ where

$$k_1 = \frac{4\pi B}{\ell_b^2} \frac{(\tau^2 - 1)^{1/2}}{\text{arctanh}(1 - \tau^{-2})^{1/2}}. \quad (8)$$

In figure 3 we show the value of k_1 determined from ABAQUS simulations for a range of values of the dimensionless pressure τ and compare it to the prediction in (8). In addition, the experimental effective stiffness, k_1 , was determined by a linear fit on all data with $w_0 < h/2$. (We shall see that (8) is only valid in the limit $w_0 \ll h$.) The dependence of the measured values of k_1 on τ is plotted with the theoretical curve and numerical points in figure 3 and show that the measured stiffness is in good agreement with that expected from the theoretical analysis. The range of pressures used in our experiments are such that the Pezzi ball is a strongly pressurized shell (i.e. $\tau \gg 1$), in which limit we find

$$k_1 \sim \frac{4\pi B}{\ell_b^2} \frac{\tau}{\log 2\tau} = \frac{\pi p R}{\log 2\tau}. \quad (9)$$

We note that for $\tau \ll 1$ we recover the unpressurized result of Reissner¹³, which in our notation reads $k_1 = 8B/\ell_b^2$. These asymptotic results are also shown in figure 3 for completeness. We also note that the result (9) is similar to that obtained from a simplified analysis of the indentation of a cylindrical cell⁸, albeit with a

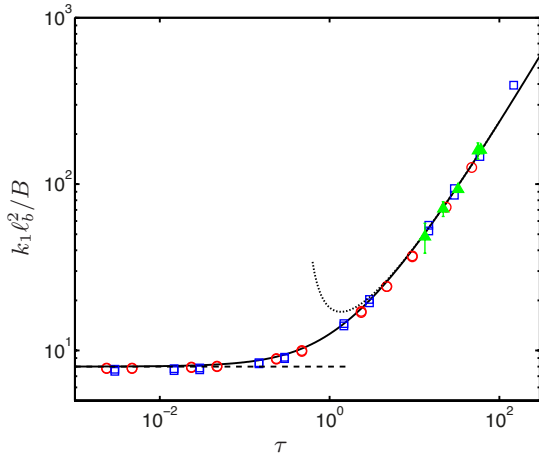


FIG. 3. (Online version in colour.) Small indentation. The dependence of the dimensionless shell stiffness $k_1 \ell_b^2 / B$ on the dimensionless pressure τ , which is defined in (7). The solid curve shows the theoretical prediction (8), which is approximated by the result of Reissner¹³, $k_1 \sim 8B / \ell_b^2$, for $\tau \ll 1$ (dashed line) and by (9) for $\tau \gg 1$ (dotted curve). Open points show the results from simulations with shell thicknesses $h = 2$ mm (blue squares) and $h = 5$ mm (red circles). All other material properties are as in fig. 2(a). Solid points (green triangles) show experimental results obtained using a Pezzi ball with error bars given by repeated trials at different loading speeds.

different prefactor. This similarity is to be expected on dimensional grounds. Finally, the force law $f = k_1 w_0$ is expected to hold provided that the effects of geometrical non-linearities are relatively small, i.e. that the first term on the RHS of (2) dominates the second term. Quantitatively, this requires that $w_0 \ll h$.

IV. LARGE INDENTATION

We now consider an indentation $w_0 \gg h$. In this regime, we must carefully account for geometrical non-linearities. Numerical simulations suggest that the force-displacement curve temporarily loses its linearity but ultimately regains it, albeit with a different stiffness, i.e. $F \sim k_2 w_0$. To understand this behaviour, it is important to consider the fully nonlinear problem described by (1)-(2). However, to simplify the analysis we neglect the effect of bending stiffness, the biharmonic term in (1). The coefficient of the bending term in (1) is a fraction τ^{-2} of the other terms and hence this approximation is valid provided that $\tau \gg 1$. With this simplification, we find that the shell equations may be integrated once and simplified to give

$$\frac{F}{2\pi} = \frac{pr^2}{2} + \psi \left(\frac{dw}{dr} - \frac{r}{R} \right) \quad (10)$$

and

$$r \frac{d}{dr} \left[\frac{1}{r} \frac{d}{dr} (r\psi) \right] = Eh \left[\frac{r}{R} \frac{dw}{dr} - \frac{1}{2} \left(\frac{dw}{dr} \right)^2 \right], \quad (11)$$

where we have used the behaviour $\psi \sim pRr/2$ as $r \rightarrow \infty$ to eliminate the constant that arises upon integrating (2). Having neglected the influence of the bending stiffness on this problem, a new length scale

$$\ell_p = \left(\frac{pR}{Eh} \right)^{1/2} R \quad (12)$$

emerges from a balance between in-plane stretching and the geometric stretching caused by the internal pressure.

We note that it is possible to transform equations (10)-(11) into a single equation for the stress function ψ by eliminating dw/dr from (11) using (10), as has been done previously for problems in planar membrane theory^{25,26}. However, here we leave the equations in the above form and solve them numerically, using the MATLAB routine `bvp4c`, subject to the boundary conditions

$$\begin{aligned} w(0) &= -w_0, \quad \lim_{r \rightarrow 0} (r\psi' - \nu\psi) = 0, \\ w(\infty) &= 0, \quad \psi'(\infty) = pR/2. \end{aligned} \quad (13)$$

The second boundary condition corresponds to the condition of zero horizontal displacement at the origin²⁷. The force F is determined as part of the solution to this problem. Its dependence on the imposed displacement w_0 is shown as the solid black curve in figure 4a and is compared to the simulation results obtained from ABAQUS, shown by the coloured curves, as well as experimental results, shown by points. This comparison shows good agreement between the theoretical result, simulations and experiment with the discrepancies accounted for by our neglect of the bending stiffness, B , in this membrane model.

Figure 4a suggests that in the limit of very large displacements we find $F \propto pRw_0$. To understand this behaviour for large forces we introduce the dimensionless force $\mathcal{F} = F/2\pi p \ell_p^2$. We also rewrite (10) by introducing dimensionless variables $\Phi = r\psi/\mathcal{F} p \ell_p^2$, $\eta = r^2/\mathcal{F} \ell_p^2$ and $\omega = wR/\mathcal{F} \ell_p^2$ to find that

$$\frac{d\omega}{d\eta} = \frac{1}{2} + \frac{1 - \eta/2}{2\Phi}, \quad (14)$$

which may then be used to rewrite (11) as

$$\frac{1}{\mathcal{F}} \frac{d^2 \Phi}{d\eta^2} = \frac{1}{8} \left[1 - \frac{(1 - \eta/2)^2}{\Phi^2} \right]. \quad (15)$$

In the limit $\mathcal{F} \gg 1$ (15) takes the usual form of a boundary layer equation with a small parameter, $1/\mathcal{F}$, multiplying the highest order derivative. Far away from the point of indentation, we expect that the LHS of (15) can be approximated by 0, giving $\Phi \approx |1 - \eta/2|$. Substituting this into (14) we find then that $\omega = 0$ for $\eta > 2$ and

$\omega = \eta - 2$ for $\eta < 2$. Upon rewriting $\omega = \eta - 2$ in dimensional terms and requiring that $w(0) = -w_0$ we find that in the limit $w_0 \gg \ell_p^2/R$ the deformation of the shell is described by

$$w = \begin{cases} -w_0 + r^2/R, & r \leq (w_0 R)^{1/2}, \\ 0, & r > (w_0 R)^{1/2}, \end{cases} \quad (16)$$

which is simply the inverted spherical cap found by Pogorelov¹⁴ for the case of unpressurized shells — also commonly known as ‘mirror buckling’. This shape is shown in rescaled form in figure 4b as the solid black curve demonstrating that the numerical solution of the membrane model (10)-(11) are well approximated by this result for $w_0 R/\ell_p^2 \gg 1$. We note that in (16) the shell is only deformed for $r < (w_0 R)^{1/2}$ — the flat regions for $r > (w_0 R)^{1/2}$ in fig. 4b indicate that the shell is not deformed in this region.

The above analysis also demonstrates that $F \sim \pi p R w_0$. Alternatively, we may understand the linear force law that is observed in this regime by noting that the decrease in volume of the shell caused by this deformation is $\Delta V \approx \pi R w_0^2/2$ and hence that the work done by the loading force in compressing the gas within the shell, $p\Delta V \approx \pi p R w_0^2/2$. Differentiating this expression with respect to w_0 we find that the applied force

$$F \sim \pi p R w_0. \quad (17)$$

The asymptotic result (17) is confirmed by the numerical solution of the membrane model (10)-(11), as shown by the dotted black line in figure 4a.

V. DISCUSSION AND APPLICATIONS

We have studied the indentation of a pressurized elastic shell and shown that the force-displacement curve exhibits two linear regimes (at small and large deflections compared to the thickness h). For strongly pressurized shells, we found that $F \sim k_1 w_0$ for $w_0 \ll h$ and $F \sim k_2 w_0$ for $w_0 \gg h$ where

$$k_1 \sim \frac{\pi p R}{\log 2\tau}, \quad k_2 \sim \pi p R, \quad (18)$$

$$\tau = \frac{1}{2} \sqrt{3(1-\nu^2)} \frac{p R^2}{E h^2} \gg 1.$$

We validated these analytical results using finite element simulations and macroscopic experiments. The analytical understanding of these two regimes gained here may be used to determine both p and $E h^2$ using data from a single indentation experiment in which both k_1 and k_2 are measured. This is in contrast to previous techniques²⁰, which required a single stiffness to be measured in two different experimental geometries in combination with numerical simulation. Our technique is particularly useful when it is the internal swelling pressure (or osmotic pressure) that is to be measured, since the result in (18)

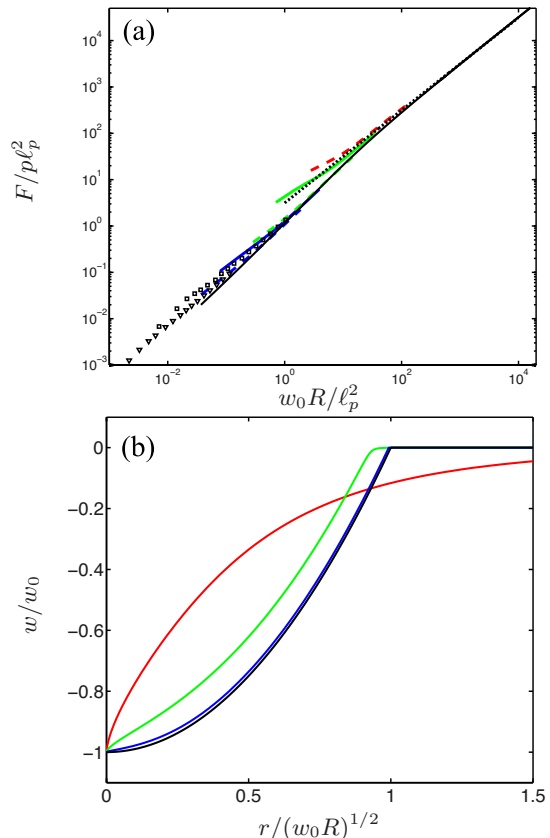


FIG. 4. (Online version in colour.) Large indentation. (a) Force F required to give an imposed displacement w_0 . The results of simulations with $R = 1$ m, $E = 70$ GPa and $\nu = 0.3$ are shown as coloured curves for different internal pressures p (blue: $p = 10$ MPa, green: $p = 1$ MPa, red: $p = 0.1$ MPa) and shell thicknesses h (dashed curves represent $h = 2$ mm, solid curves $h = 5$ mm). The solid black curve gives the membrane prediction obtained by solving (10)-(11) while the dotted black line gives the asymptotic result (17). The experimental results of fig. 2b are also shown for $p = 1.2$ kPa (squares) and $p = 5.4$ kPa (triangles). (b) Rescaling of the deformation profile suggested by (16). The numerical results of the membrane model for $w_0 R/\ell_p^2 = 1$ (red), 10^2 (green) and 10^4 (blue) demonstrate that for $w_0 R/\ell_p^2 \gg 1$ we recover the inverted spherical cap profile (16), shown as the solid black curve.

shows that the stiffness k_2 depends only on this pressure and the radius of the capsule. We note that the experiments of Gordon *et al.*²⁰ appear to be precisely in this regime since, using their estimates, the parameter $w_0 R/\ell_p^2 \sim 100 \gg 1$. Using the asymptotic result (18) we find that their experimental data suggests internal pressures ranging from 15 Pa to 120 Pa (assuming a capsule radius of 100 μ m). This is in reasonable agreement with the values given by them (100 – 500 Pa) but is less sensitive to errors in fitting since it is not necessary to estimate the elastic properties of the shell as well.

Our results may also be applied to understand recent experiments²² on yeast cells, *Saccharomyces cerevisiae*, in which indentation with an AFM tip was used to de-

termine changes in the cell's stiffness as the osmotic pressure of the external medium was varied. These experiments were performed for indentations on the order of the wall thickness (maximum indentation ≈ 50 nm compared to a typical wall thickness⁶ $h \approx 70$ nm) and hence the measured stiffness corresponds to k_1 in our notation. The cell wall of yeast is known to be permeable allowing material to flow out of the cell and equilibrate non-osmotic pressure differences²⁸. Although this flow could in principle be modelled²⁸, the relatively small size of indentations, together with the experimental observation that results are unchanged upon varying the indentation speed, suggest that the assumption made in our analysis of constant pressure difference during indentation is satisfactory. Other complications include the layered structure of the yeast cell wall, with not all layers contributing equally to its mechanical strength²⁹, and the potentially complicated constitutive law relating stresses and strains. Nevertheless, the application of the theoretical understanding developed from the idealised model presented in this paper gives us a starting point for extracting characteristic moduli and values for the internal osmotic pressure.

The principle result of the indentation experiments of Arfsten *et al.*²² is that the value of k_1 depends on the osmotic pressure of the external medium (see figure 5a). Furthermore, they found that above a critical external osmotic pressure, $P_{ext} = 2.1$ MPa, this stiffness becomes significantly smaller. From this observation it was concluded that the cell is effectively deflated when $P_{ext} = 2.1$ MPa and hence that the internal osmotic pressure of the cell is $P_{int} = 2.1$ MPa. Strictly speaking, this value is the maximal osmotic pressure that the cell can generate. Our analysis suggests that, as the pressure difference decreases, a residual stiffness should remain and be explained by the analysis of Reissner¹³. Using this result and typical estimates for the thickness of the cell wall $h \approx 70$ nm and cell radius $R \approx 2.75$ μ m from the literature⁶ we take the measured upper and lower bounds for k_1 (see dashed lines in figure 5a) and estimate that 12 MPa $\leq E \leq 46$ MPa. This value is reasonably consistent with values determined previously^{5,31} and also gives $\ell_p \approx 2$ μ m and $\ell_b \approx 200$ nm, which are both significantly larger than the AFM tip used ($\lesssim 15$ nm) justifying our approximation of a point force. With this value of E , the theory developed here, more specifically Eq.(8), can be used to estimate the internal pressure required to obtain the observed values of k_1 . The results of this calculation are shown in figure 5b and indicate that as the external pressure is increased so the internal pressure is actively increased to maintain a certain degree of turgor, i.e. an internal osmotic pressure that is higher than that of the external medium. Beyond $P_{int} = 0.6$ MPa the cell becomes unable to maintain turgor.

We find a typical value of turgor of 0.1–0.2 MPa, which is consistent with experiments using different methodologies^{30,31}, which found turgor pressures in the range 0 – 1 MPa. Finally, we note that for these exper-

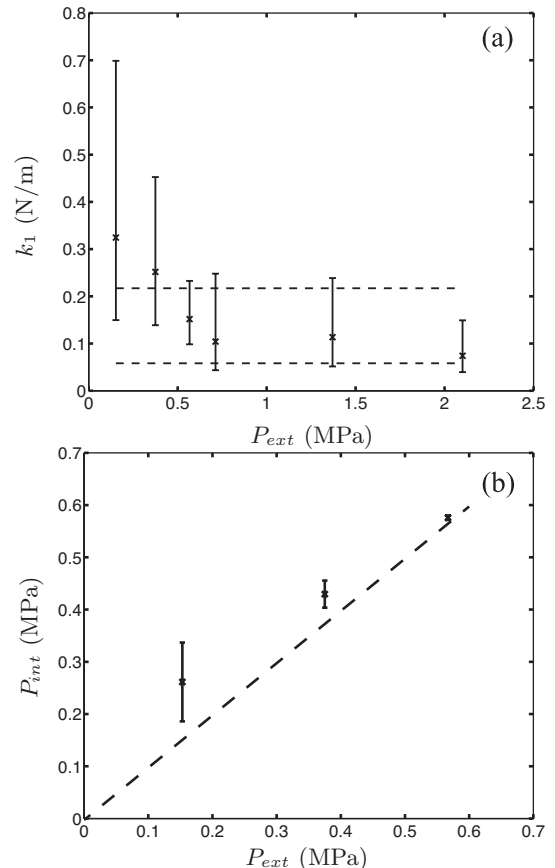


FIG. 5. (a) Raw results of measurements of k_1 for yeast cells in media of different osmotic pressure reported previously²². Measurements over many cells were found to follow a log-normal distribution and hence were summarized by the median value (crosses) and the 68.3%-confidence interval, corresponding to one standard deviation, for $\log k_1$ (error bars)²². Dashed lines show the minimum and maximum values of k_1 taken to estimate the Young's modulus E , see text. (b) Dependence of the internal pressure of these yeast cells on the external osmotic pressure based on the results of this paper. Here we have used the data at larger external pressure to determine the Young's modulus of the cell wall and then to estimate the pressure difference felt by the cell at lower external osmotic pressures thereby inferring the internal pressure.

iments $0 \lesssim \tau \lesssim 10$ and so it is necessary to make use of the full analytical expression (8). This is particularly important for explaining the presence of a residual stiffness when the yeast cell is unable to maintain turgor (for external pressures $P_{ext} \gtrsim 0.6$ MPa). As Arfsten *et al.* surmised²², the presence of this stiffness demonstrates that the role of bending effects cannot be neglected as turgor decreases — an assumption that is often made in simplified models of cell indentation^{8,9}.

We anticipate that our analytical results, and particularly the asymptotic results (18) for strongly pressurized shells, could provide a standard tool for the mechanical characterization of pressurized shells in a range of biological applications, such as the measurement of the

properties of capsules and walled cells. Other features of the indentation of pressurized shells may also aid this aim. For example, under large deformations pressurized shells are subject to an azimuthal buckling instability that leads to the formation of a large number of wrinkles with a well-defined length. The number of wrinkles as well as their length could thus be used for the mechanical characterization of shells^{32,33}. A full study of this wrinkling is currently underway.

ACKNOWLEDGMENTS

D.V. was supported by an Oppenheimer Early Career Fellowship. This publication is based on work sup-

ported in part by Award No. KUK-C1-013-04, made by King Abdullah University of Science and Technology (KAUST). A.A. and A.V. are thankful for the support of NSF CMMI grant award #1065759. A.B. was supported by ANR - BLANC - Mechastem. We are grateful to Mark Hallworth and Sébastien Moulinet for their assistance with the experimental aspects, and to Mokhtar Adda-Bedia for encouragement and for laboratory space.

-
- ¹ Sneddon, I. N. 1965 The relation between load and penetration in the axisymmetric Boussinesq problem for a punch of arbitrary profile. *Int. J. Eng. Sci.* **3**, 47–57.
 - ² Cheng, Y.-T. & Cheng, C.-M. 2004 Scaling, dimensional analysis, and indentation measurements. *Mater. Sci. Eng. R.* **44**, 91–149.
 - ³ Hu, Y., Zhao, X., Vlassak, J. J. & Suo, Z. 2010 Using indentation to characterize the poroelasticity of gels. *Appl. Phys. Lett.* **96**, 121904.
 - ⁴ Pelling, A. E., Sehati, S., Gralla, E. B., Valentine, J. S. & Gimzewski, J. K. 2004 Local nanomechanical motion of the cell wall of *Saccharomyces cerevisiae*. *Science* **305**, 1147–1150.
 - ⁵ Smith, A. E., Zhang, Z., Thomas, C. R., Moxham, K. E. & Middelberg, A. P. J. 2000 The mechanical properties of *Saccharomyces cerevisiae*. *Proc. Natl. Acad. Sci. USA* **97**, 9871–9874.
 - ⁶ Srinorakutara, T. 1998 Determination of yeast cell wall thickness and cell diameter using new methods. *J. Ferment. Bioeng.* **86**, 253–260.
 - ⁷ Corson, F., Hamant, O., Bohn, S., Traas, J., Boudaoud, A. & Couder, Y. 2009 Turning a plant tissue into a living cell froth through isotropic growth. *Proc. Natl. Acad. Sci. USA* **106**, 8453–8458.
 - ⁸ Arnoldi, M., Fritz, M., Bäuerlein, E., Radmacher, M., Sackmann, E. & Boulbitch, A. 2000 Bacterial turgor pressure can be measured by atomic force microscopy. *Phys. Rev. E* **62**, 1034–1044.
 - ⁹ Boulbitch, A. A. 2000 Deformation of the envelope of a spherical Gram-negative bacterium during the atomic force microscopic measurements. *J. Electron Microsc.* **49**, 459–462.
 - ¹⁰ Yao, X., Walter, J., Burke, S., Stewart, S., Jericho, M. H., Pink, D., Hunter, R. & Beveridge, T. J. 2002 Atomic force microscopy and theoretical considerations of surface properties and turgor pressures of bacteria. *Colloid Surface B* **23**, 213–230.
 - ¹¹ Wan, K.-T., Chan, V. & Dillard, D. A. 2002 Constitutive equation for elastic indentation of a thin-walled biomimetic microcapsule by an atomic force microscope tip. *Colloid Surface B* **27**, 241–248.
 - ¹² Reissner, E. 1947 Stresses and small displacements of shallow spherical shells, I. *J. Math. Phys.* **25**, 80–85.
 - ¹³ Reissner, E. 1947 Stresses and small displacements of shallow spherical shells, II. *J. Math. Phys.* **25**, 279–300.
 - ¹⁴ Pogorelov, A. V. 1988 *Bending of Surfaces and Stability of Shells* (AMS Bookstore, Providence, RI).
 - ¹⁵ Wierzbicki, T. & Suh, M. S. 1988 Indentation of tubes under combined loading. *Int. J. Mech. Sci.* **30**, 229–248.
 - ¹⁶ Vaziri, A. & Mahadevan, L. 2008 Localized and extended deformations of elastic shells. *Proc. Natl. Acad. Sci. USA* **105**, 7913–7918.
 - ¹⁷ Vaziri, A. 2009 Mechanics of highly deformed elastic shells. *Thin Wall. Struct.* **47**, 692–700.
 - ¹⁸ Gere, J. M. & Godono, B. J. 2009 *Mechanics of Materials* (Cengage, Toronto).
 - ¹⁹ Tsapis, N., Bennett, D., Jackson, B., Weitz, D. A. & Edwards, D. A. 2002 Trojan particles: Large porous carriers of nanoparticles for drug delivery. *Proc. Natl. Acad. Sci. USA* **99**, 12001–12005.
 - ²⁰ Gordon, V. D., Chen, X., Hutchinson, J. W., Bausch, A. R., Marquez, M. & Weitz, D. A. 2004 Self-assembled polymer membrane capsules inflated by osmotic pressure. *J. Am. Chem. Soc.* **126**, 14117–14122.
 - ²¹ Taber, L. A. 1982 Large deflection of a fluid-filled spherical-shell under a point load. *J. Appl. Mech.* **9**, 121–128.
 - ²² Arfsten, J., Leupold, S., Bradtmöller, C., Kampen, I. & Kwade, A. 2010 Atomic force microscopy studies on the nanomechanical properties of *Saccharomyces cerevisiae*. *Colloids Surf. B: Biointerfaces* **79**, 284–290.
 - ²³ Shipman, P. 2004 Ph.D. thesis (University of Arizona, USA).
 - ²⁴ Abramowitz, M. & Stegun, I. A. 1964 *Handbook of Mathematical Functions with Formulas, Graphs, and Mathematical Tables* (Dover, New York).
 - ²⁵ Chopin, J., Vella, D. & Boudaoud, A. 2008 The liquid blister test. *Proc. R. Soc. London A* **464**, 2887–2906.
 - ²⁶ Vella, D., Adda-Bedia, M. & Cerda, E. 2010 Capillary wrinkling of elastic membranes. *Soft Matter* **6**, 5778–5782.
 - ²⁷ Timoshenko, S. P. & Woinowsky-Krieger, S. 1959 *Theory of Plates and Shells* (McGraw-Hill, Singapore).
 - ²⁸ Smith, A. E., Moxham, K. E. & Middelberg, A. P. J. 1998 On uniquely determining cell-wall material properties with the compression experiment. *Chem. Eng. Sci.* **53**, 3913–3922.

- ²⁹ Klis, F. M., Boorsma, A. and de Groot, P. W. J. 2006 Cell wall construction in *Saccharomyces cerevisiae*. *Yeast* **23**, 185–202.
- ³⁰ Minc, N., Boudaoud, A. & Chang, F. 2009 Mechanical forces of fission yeast growth. *Curr. Biol.* **19**, 1096–1101.
- ³¹ Schaber, J., Adrover, M. A., Eriksson, E., Pelet, S., Petelenz-Kurdziel, E., Klein, D., Posas, F., Goksör, M., Peter, M., Hohmann, S. & Klipp, E. 2010 Biophysical properties of *Saccharomyces cerevisiae* and their relationship with HOG pathway activation. *Eur. Biophys. J.* **39**, 1547–1556.
- ³² Huang, J., Juskiewicz, M., de Jeu, W. H., Cerda, E., Emrick, T., Menon, N. & Russell, T. P. 2007 Capillary wrinkling of floating thin polymer films. *Science* **317**, 650–653.
- ³³ Bernal, R., Tassuis, Ch., Melo, F. & Géminard, J.-Ch. 2011 Elastic response and wrinkling onset of curved elastic membranes subjected to indentation test. *Eur Phys. J. E* **34**, 13.

RECENT REPORTS

08/11	Hysteresis and Post Walrasian Economics	Cross McNamara Kalachev Pokrovskii
09/11	A locally adaptive time-stepping algorithm for petroleum reservoir simulations	McNamara Bowen Dellar
10/11	On the predictions and limitations of the BeckerDoring model for reaction kinetics in micellar surfactant solutions	Griffiths Bain Beward Colegate Howell Waters
11/11	Dynamics of the Tear Film	Braun
12/11	The influence of receptor-mediated interactions on reaction-diffusion mechanisms of cellular self-organisation	Klikaa Baker Headon Gaffney
13/11	Quasi-steady state analysis of two-dimensional random intermittent search processes	Bressloff Newby
14/11	A Constrained Approach to Multiscale Stochastic Simulation of Chemically Reacting Systems	Cotter Zygalakis Kevrekidis Erban
15/11	The Two Regime Method for optimizing stochastic reaction-diffusion simulations	Flegg Chapman Erban
16/11	Recombination via tail states in polythiophene:fullerene solar cells	Kirchartz Pieters Kirkpatrick Rau Nelson
17/11	Energy versus electron transfer in organic solar cells: a comparison of the photophysics of two indenofluorene: fullerene blend films	Soon Clarke Zhang Agostinelli Kirkpatrick Dyer-Smith McCulloch Nelson Durrant
18/11	Asymptotic analysis of a pile-up of edge dislocation	Hall
19/11	A perturbation analysis of spontaneous action potential initiation by stochastic ion channels	Keener1 Newby
20/11	Hybrid modelling of individual movement and collective behaviour	Franz Erban

23/11	Positive or negative Poynting effect? The role of adscititious inequalities in hyperelastic materials	Mihai Goriely McCue McElwain
24/11	On approaches to modelling lattice dislocations	Hall Markenscoff
25/11	Nonlinear waves in heterogeneous elastic rods via homogenization	de Luna Emptage Goriely Bressloff
26/11	Synaptic bistability due to nucleation and evaporation of receptor clusters	Burlakov Duričković Goriely
27/11	Particle trapping and banding in rapid solidification	Elliot Peppin
28/11	Growth of confined cancer spheroids: a combined experimental and mathematical modelling approach	Loessner Flegg Byrne Hall Moroney Clements McElwain Hutmacher
29/11	Floating carpets and the delamination of elastic sheets	Wagner Vella
30/11	Numerical Study of Liquid Crystal Elastomers by a Mixed Finite	Luo Calderer

Copies of these, and any other OCCAM reports can be obtained from:

**Oxford Centre for Collaborative Applied Mathematics
Mathematical Institute
24 - 29 St Giles'
Oxford
OX1 3LB
England
www.maths.ox.ac.uk/occam**